Chapter 10

Super-Resolution Microscopy of the Neuronal Calcium-Binding Proteins Calneuron-1 and Caldendrin

Johannes Hradsky, Marina Mikhaylova, Anna Karpova, Michael R. Kreutz, and Werner Zuschratter

Abstract

Calcium (Ca^{2+}) signaling in neurons is mediated by plethora of calcium binding proteins with many of them belonging to the Calmodulin family of calcium sensors. Many studies have shown that the subcellular localization of neuronal EF-hand Ca^{2+}-sensors is crucial for their cellular function. To overcome the resolution limit of classical fluorescence and confocal microscopy various imaging techniques have been developed recently that improve the resolution by an order of magnitude in all dimensions. This new microscope techniques make co-localization studies of Ca^{2+}-binding proteins more reliable and help to get insights into the macromolecular organization of intracellular structures and signaling pathways beyond the diffraction limit of visible light.

Key words: STED microscopy, Synaptic proteins, Cytoskeleton, Golgi apparatus, Calneuron, Caldendrin, Calcium, EF-hand

1. Introduction

1.1. Compartmentalization of Ca^{2+} Signaling in Neurons and Role of Calmodulin-Like Neuronal Calcium-Binding Proteins

Ca^{2+} signaling in neurons exhibits steep spatiotemporal gradients with a spatial resolution of micro- and nanodomains (1, 2). Occurrence of Ca^{2+} gradients is strongly related to Ca^{2+} influx from extracellular space or induced cytosolic release from intracellular stores (endoplasmic reticulum/ER, Golgi complex, and other). Gradients derived from sequestration of Ca^{2+} ions by ER, mitochondria, and locally enriched Ca^{2+} buffer proteins can be generated (2, 3). Multiple Ca^{2+} sensor proteins play a crucial role

Johannes Hradsky and Marina Mikhaylova have contributed equally to the work.

Claus W. Heizmann (ed.), *Calcium-Binding Proteins and RAGE: From Structural Basics to Clinical Applications*, Methods in Molecular Biology, vol. 963, DOI 10.1007/978-1-62703-230-8_10, © Springer Science+Business Media New York 2013

in transducing Ca^{2+} signals into alterations of cellular processes. Especially a large variety of Calmodulin-like Ca^{2+}-binding proteins is expressed in the central nervous system. The groups of neuronal calcium sensors (NCS) and neuronal calcium-binding proteins (nCaBPs) derived from their ancestor Calmodulin gave rise a variety of proteins that exhibit different Ca^{2+}-binding properties, tissue, cell type, and subcellular localization profiles (see ref. 4 for review).

Calmodulin (CaM) is a very abundant small cytosolic protein that can be recruited to the different neuronal compartments via interaction with its protein targets (5). Differently from CaM, NCS proteins are associated with intracellular membranes via co-translational N-terminal lipid modification by myristoyltransferase (NCS-1, Hippocalcin, Recoverin, KChIPs, VILIPs, and others) (4, 6). A Ca^{2+}-induced myristoyl switch triggers the conformational changes and membrane recruitment of some NCS proteins (Recoverin, VILIPs (4, 7)). nCaBP proteins also can be *N*-myristoylated (like s- and l-CaBP1) but additionally, adopt different strategies for targeting to a particular cell compartment. For example, Calneuron-1 and Calneuron-2 (also called CaBP8 and CaBP7, respectively) are unique members of nCaBP group because their targeting to Golgi membranes and post-Golgi vesicular compartments is provided by the C-terminal transmembrane domain (TMD) (8–11). Interestingly, they are the only members of EF-hand protein superfamily that can be classified as tail-anchored proteins (9, 11). Calneurons are initially post-translationary inserted into the endoplasmic reticulum (ER) with assistance of TRC40/ASNA1 chaperon and then, due to the length of the TMD and associations with particular phospholipids, are transported to the Golgi complex (11). Calneurons are enriched at the Golgi but they also can be found along the constitutive secretory pathway and at the plasma membrane (9–11). At the Golgi network, Calneurons decode local calcium concentrations via regulating the activity of phosphatidylinositol 4-kinase IIIβ (PI-4KIIIβ), thus providing a Ca^{2+}-dependent control for the regulated local synthesis of phosphatidylinositol 4-phosphate (PI(4)P) and for the exit of vesicles from the trans-Golgi network (4, 10, 12). At the plasma membrane of bovine chromaffin cells, Calneuron-1 is involved in transduction of Ca^{2+} signaling and regulating the activity of voltage gated Ca^{2+} channels (VGCC) (13). A mutant Calneuron-1 lacking the C-terminal transmembrane domain did not inhibit currents generated through N-, L-, and P/Q-type channels indicating that proper targeting of Calneuron-1 is required for its function (13). Caldendrin is a founding member of nCaBP group of Ca^{2+}-sensors. Caldendrin is abundant in brain where it shows prominent immunostaining of the neurons in the cortex, hip-

pocampus, and hypothalamus (14–16). Caldendrin is enriched in somatodendritic compartments and is enriched in the postsynaptic density fraction after induction of kainate-induced seizures (17). In terms of its EF-hand organization, Caldendrin/CaBP1 is the closest homologue of CaM in brain (14, 18, 19). Caldendrin can sense Ca^{2+} in the same dynamic range as CaM and it has, like CaM, two independent EF-hand domains connected via a linker. Differently from CaM, Caldendrin has an extended amino-terminus enriched in basic amino acids. Another important difference between Caldendrin and CaM relates to amino acid substitutions within the second EF-hand loop that render this motif incapable of Ca^{2+}-binding (14). Interestingly, CaM cannot substitute Caldendrin in terms of its interactions. Binding of Caldendrin to IP3 receptors and L-type Ca^{2+} channels ($Ca_v1.2$) modulate the properties of these channels in Ca^{2+}-dependent manner. Binding of Caldendrin, but not of CaM, has been demonstrated for the light chain 3 of microtubule-associated protein MAP1A/B (20) and for the synapto-nuclear messenger protein Jacob (21). Additionally, the amino-terminus of Caldendrin contains proline-rich regions that could serve as an interface for binding of SH3-domain proteins (4). Visualization of the precise subcellular localization of NCS and nCaBPs is important to appreciate their function. Additionally, dynamic aspects of this localization, like transport along the secretory trafficking pathway for Calneurons or activity-induced synaptic redistribution of Caldendrin can be addressed by using high-resolution light microscopy.

1.2. High-Resolution Light-Microscopy Beyond the Diffraction Limit

During the past two decades the traditional fluorescence microscopy has developed from a discipline interested in the description of static microstructures to a tool of molecular cell biology aiming to analyze physiologically relevant molecular processes on the cellular and systems network level. Exploring the function of macromolecular networks and the Ca^{2+}-mediated effects on the cellular machinery requires high-resolution microscope techniques that allow image acquisition below the diffraction limit of visible light (22). In the past, subcellular localizations of immunostained structures were only possible by time-consuming electron microscopy.

With the introduction of new optical techniques like 4pi (23), Structured Illumination (SIM) (24, 25), Spatial Illumination Microscopy (SMI) (26), Spectral-Precision-Distance Microscopy (SPDM) (27, 28), Ground State Depletion Microscopy (GSD) (29), Stimulated Emission Depletion (STED) (30, 31) or Photoactivated Localization Microscopy (PALM/STORM) (32, 33) a significant improvement of spa-

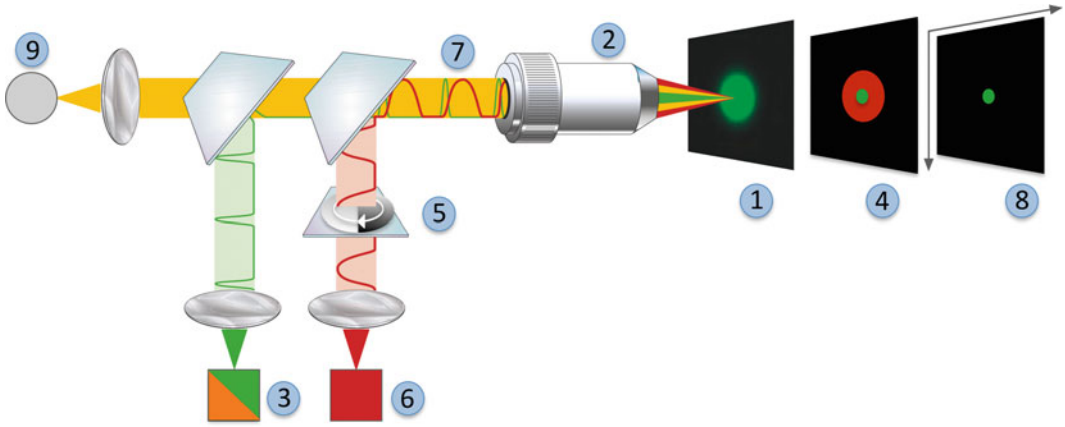

Fig. 1. Principle of STED resolution enhancement. In a conventional confocal laser scanning microscope, the sample is sequentially illuminated by a diffraction limited spot (1) via a high numerical aperture objective (2). In a Ti-Sapphire-based STED microscope, this illumination spot (produced by a pulsed excitation laser (3) of 532 or 640 nm) is overlayed by a perfectly aligned doughnut-shaped second laser pulse of 750 nm (4) produced by a Vortex phase filter (5) in the beam-path of the Ti-Sapphire depletion laser (6). The STED laser pulse immediately follows the excitation pulse with a short delay (7). As result, the excited molecules, in the doughnut-shaped area, return to the ground state without emitting spontaneous fluorescence. Because the excited molecules in the center remain unaffected from the depletion process the effective illumination spot becomes smaller (8). The power of the depletion laser (6) determines the size of the central area from where fluorescence can still be detected (9). In other words, the resolution increases with the power of the depletion laser. Diagram courtesy of Leica Microsystems, Germany.

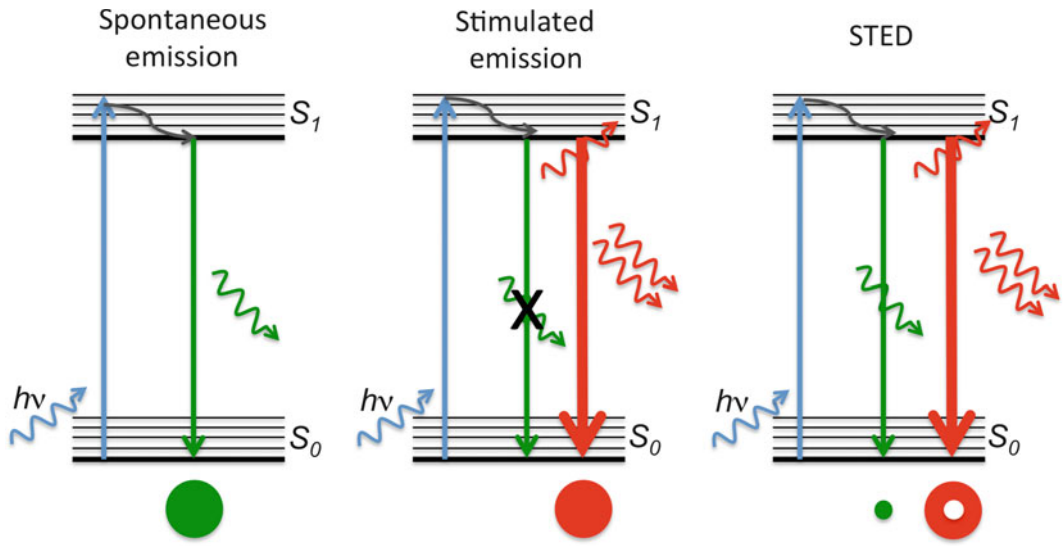

Fig. 2. Principle of spontaneous fluorescence and stimulated (induced) fluorescence emission. Spontaneous emission (*left panel*): When a fluorescent molecule absorbs light quanta, it will go to a higher energy level. From here, it will relax back spontaneously to the ground state after a short period of time (i.e., the fluorescence lifetime) by emitting a photon of less energy (i.e., red-shifted wavelength). The emission results in a diffraction limited spot. Stimulated emission (*center panel*): From the excited state a fluorescent molecule can be forced to return back to the ground state, when the electron in the excited state is stimulated by another photon, whose energy matches the difference between the electron's energy and the ground state. In this case the electron will not relax spontaneously, but will immediately return to the ground state by emitting an additional photon of the same wavelength as the incident photon. *Right panel*: In a STED microscope spontaneous fluorescence emission is restricted to the inner area of an excitation spot, whereas stimulated emission depopulates the excited molecules in an outer ring.

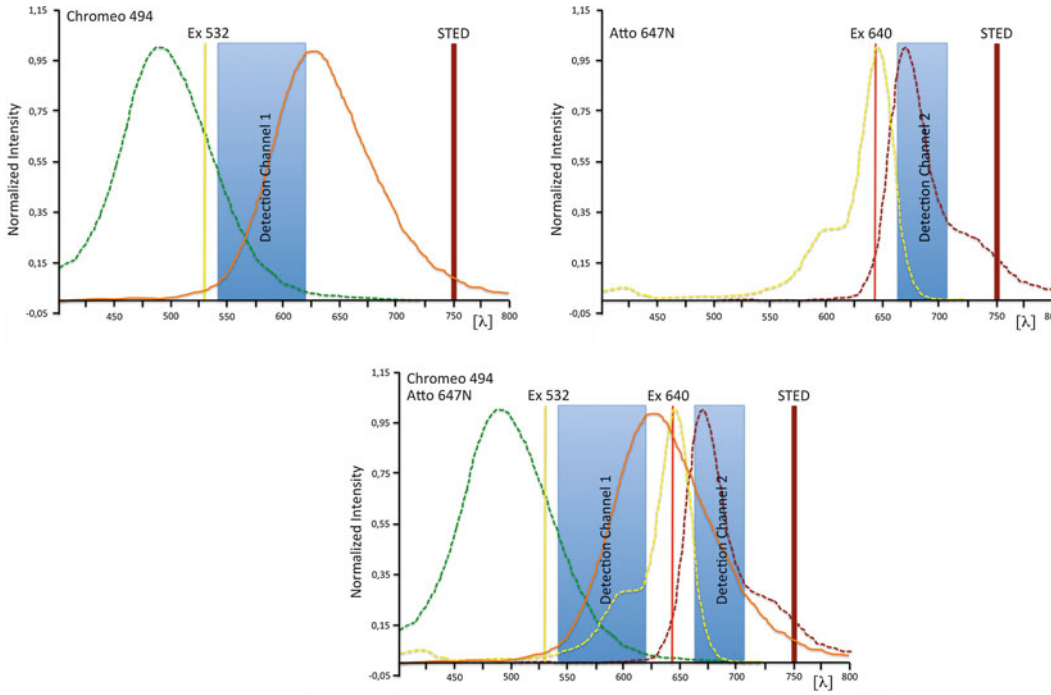

Fig. 3. Absorption and Emission spectra of Chromeo 494 (*left*) and Atto 647N (*right*) in relation to the excitation wavelength, the detection bandwidth and the depletion (STED) laser pulse. The *bottom graph* summarizes the situation in a Ti-Sapphire 2-channel STED microscope.

tial, i.e., structural resolution beyond the diffraction limit of classical microscopy (defined by Ernst Abbe in 1873 (34)) was recently achieved. Most of these concepts take advantage of the fact that fluorescence can be switched between a dark state and a bright state, either in a stochastic (PALM/STORM/GSD) or in a deterministic way (STED).

Here, we show by using two channel STED microscopy (see Notes 1 and 3, Figs. 1–3) that the subcellular distribution of the calcium-binding proteins, Calneuron and Caldendrin, can be determined with much higher precision than before (Figs. 4–8). In immunocytochemical co-localization studies, we demonstrate distinct labeling patterns of these Ca^{2+}-binding proteins along Golgi-membranes (Figs. 4 and 5), cytoskeleton-markers (Figs. 4, 5, 8) and in relation to pre- and postsynaptic scaffolding proteins (Figs. 6–8), which previously could not be resolved.

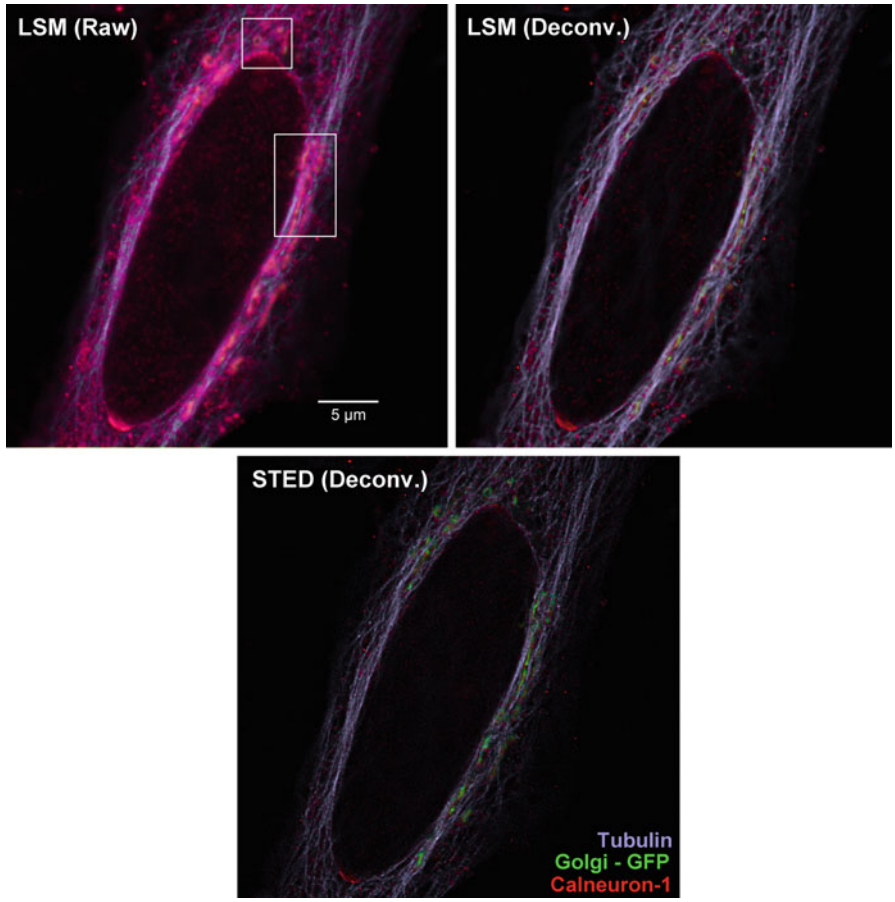

Fig. 4. HeLa and Cos7 cells were successfully transfected with the untagged Calneuron-1 construct (in pcDNA3.1) and GFP-Sec61β or GFP-Monomeric-Golgi. Subsequently, cell cultures were incubated with antibodies against β-Tubulin III and Calneuron-1 and stained using Chromeo 494 and Atto 647N as dyes suitable for Ti-Sapphire-based STED imaging. Series of STED and confocal images were taken from triple stained cells according to above protocol. Figure shows the difference between the confocal (*left panel*) and the STED (*bottom panel*) image of a HeLa cell stained with Chromeo 494 (*blue*, indicating β-Tubulin III), Atto 647N (*red*, indicating Calneuron-1) and GFP-monomeric-Golgi (*green*). Whereas the deconvolved confocal image (*right panel*) already demonstrates some optimization of the blurred confocal raw image (*left*), a significant improvement of the tubular cytoskeleton and the Calneuron-1 immunostainings becomes visible only in the STED image (*bottom*). Scale bar indicates 5 µm.

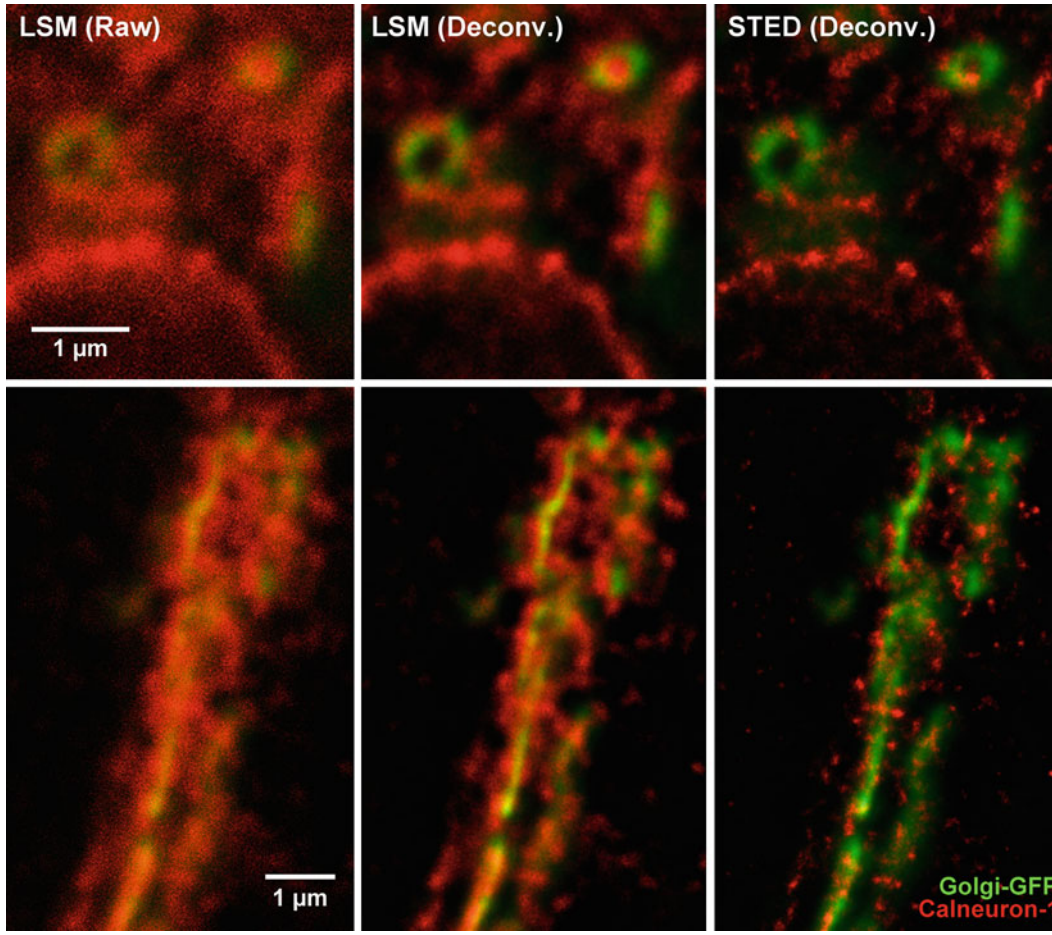

Fig. 5. Detail magnifications of the GFP-labeled Golgi apparatus (*green*) and Calneuron-1 (*red*) depicted in Fig. 10.4. The details revealed distinct foci of Calneuron-1 association along the Golgi-network (*green*) in the picture acquired in STED mode (*right panel*). In contrast to the STED-image scans recorded in the classical confocal mode (*left and center panel*) did not show such details but appeared mainly blurred due to their lower resolution. Deconvolution of the confocal raw image (*left panel*) uncovered some more details (*center panel*) but could not compete with the resolution of the STED image (*right panel*). For instance, as it would be expected, Calneuron-1 staining was mostly associated with the Golgi membrane from cytosolic leaflet but not inside of the Golgi lumen (STED images, *right panel*). Scale bar indicates 1 µm.

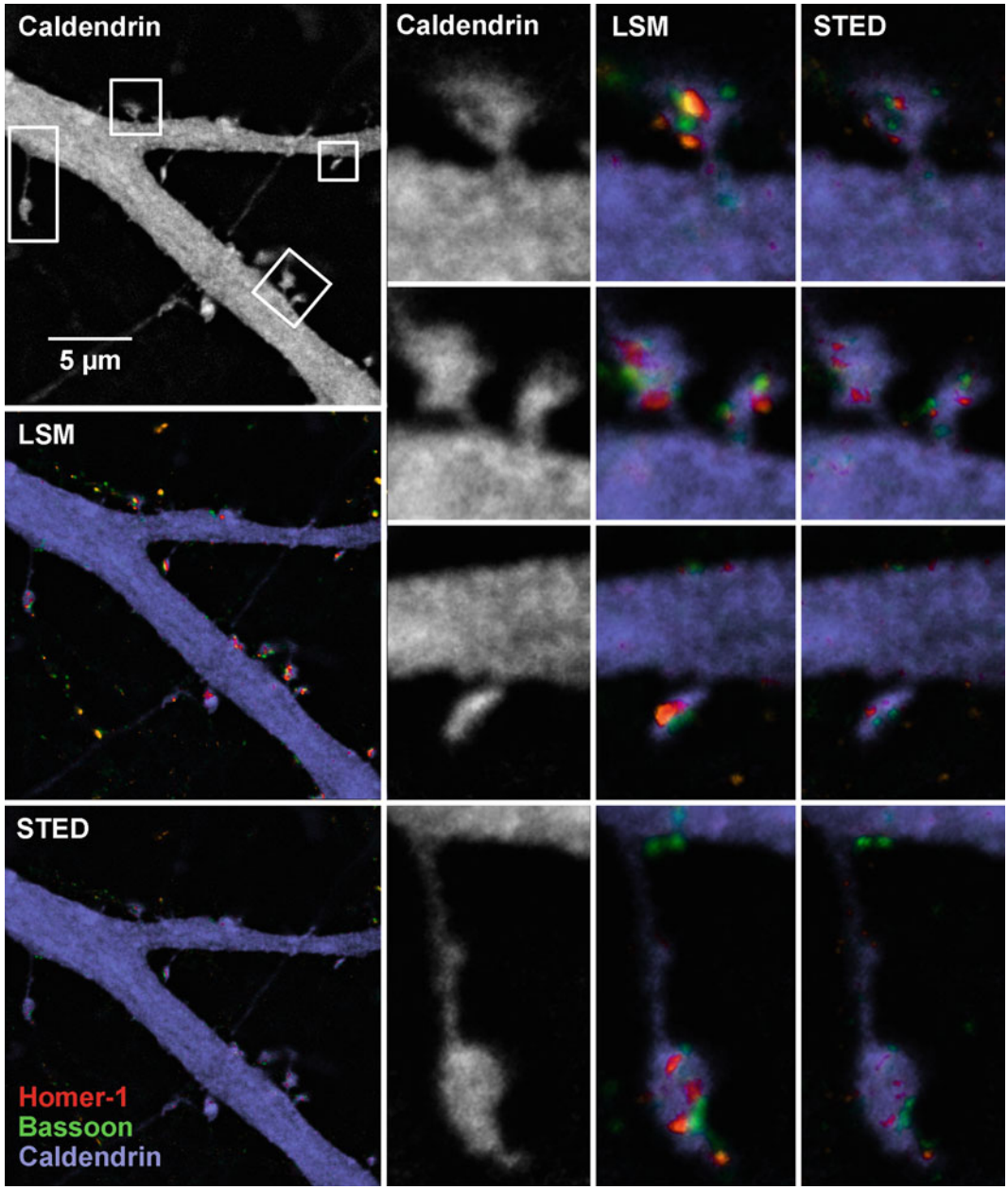

Fig. 6. To demonstrate the potential of STED imaging for characterizing the dynamics of calcium-binding proteins in neurons, we performed immunostainings against the pre- and postsynaptic scaffolding proteins, Bassoon and Homer-1, in hippocampal cell cultures, previously transfected with a GFP-fusion construct of Caldendrin. The dendritic branch of a neuron transfected with Caldendrin-GFP (*blue*) shows specific localizations of Bassoon (*green*) and Homer (*red*) mainly at spiny synapses of different size and morphology. Caldendrin is present within spines where it co-localizes with Homer. Comparison between confocal (*center panels*) and STED (*right panel*) images show that blurred structures of confocal images can be resolved as distinct contact zones within the STED images. Scale bar indicates 5 µm.

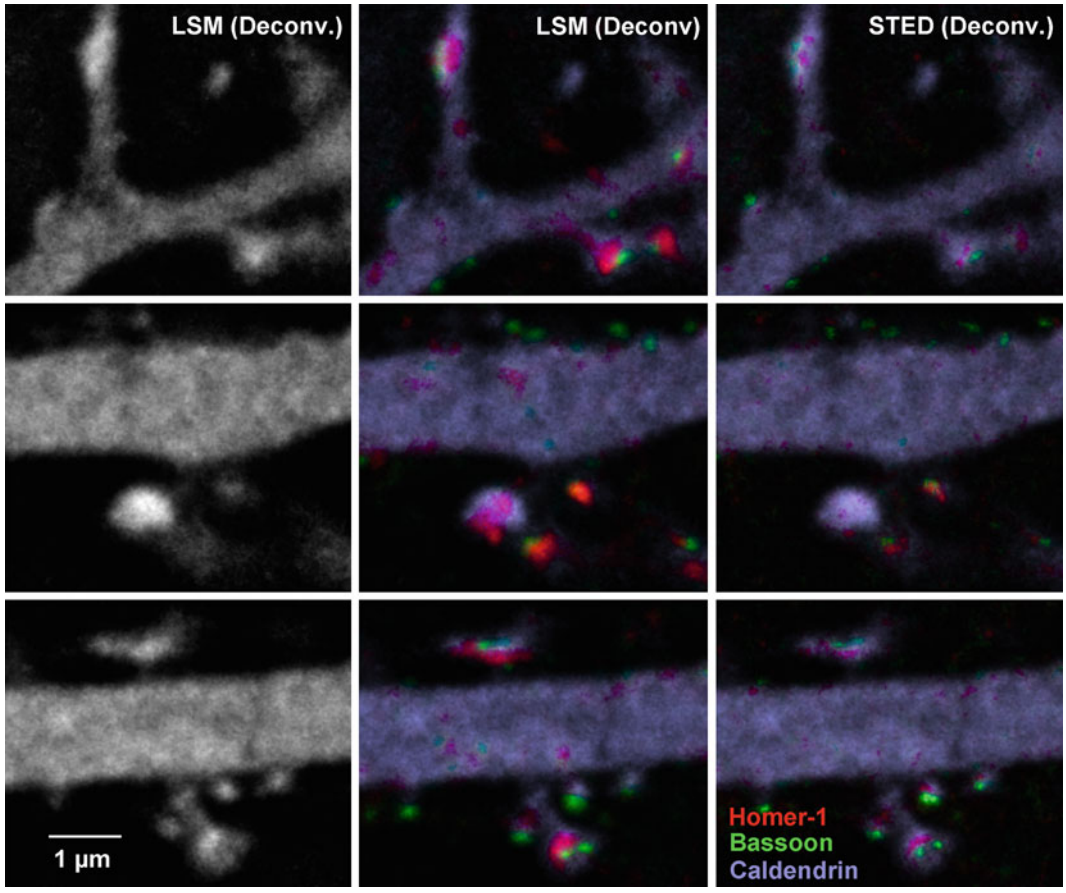

Fig. 7. Another example of Bassoon (*green*) and Homer-1 (*red*) immune-positive contacts at spines of a Caldendrin-GFP transfected cell (*blue*). Whereas some of the spiny contacts displayed an irregular or complementary distribution of Caldendrin, others exhibited a strong enhancement of the calcium-binding protein, which then correlated with the distribution of Homer. This might indicate a correlation in the activity levels of single synapses. Comparison between confocal (*left*, *center panels*) and STED (*right panel*) images revealed a more precise distribution and higher resolution of both synaptic markers in the STED images. Frequently, blurred structures of confocal images could be resolved as distinct contact zones within the STED images. Scale bar indicates 1 µm.

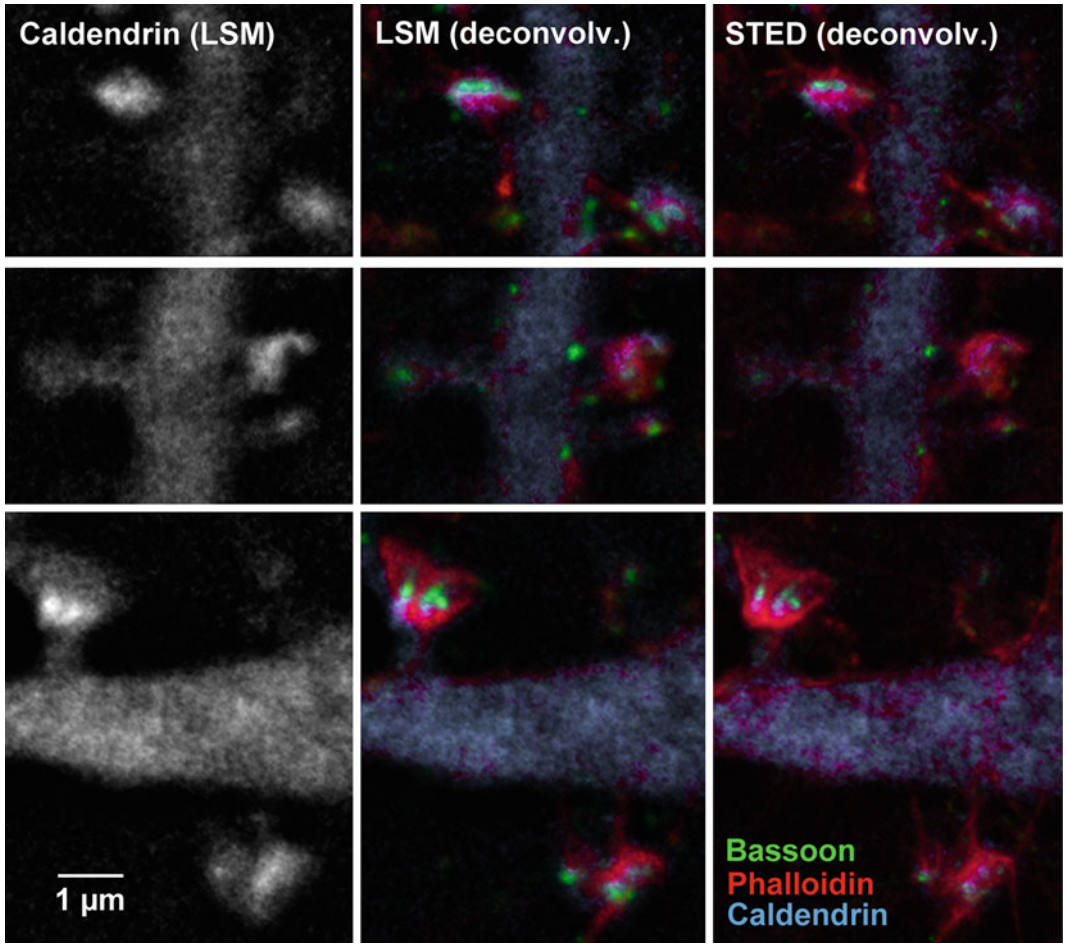

Fig. 8. To analyze the interaction of Caldendrin (*blue*) with the actin-cytoskeleton we exchanged Homer antibody-staining by Phalloidin-Atto 647N (*red*) incubation. STED imaging (*right*) showed that Caldendrin (*blue*) is rather complementary or associated than fully overlapping with Phalloidin (*red*) staining. Again the STED images (*right*) showed a considerable higher resolution in which individual contact zones of the presynaptic marker Bassoon (*green*) could be distinguished. Scale bar indicates 1 µm.

2. Materials

2.1. Cell Culture and Transfection Reagents

1. NB medium → Neurobasal® Medium (Gibco).
2. NB(−) → NB, 1× B27 (Gibco), 0.5 mM l-Glutamine.
3. NB(+) → NB(−), 100 U/mL Penicillin.
4. Opti-MEM® *Reduced Serum Medium* (Gibco).
5. DMEM → Dulbecco's Modified Eagle Medium (Gibco).
6. DMEM(+) → DMEM, 10% fetal calf serum (FCS), 2 mM l-glutamine, 100 U/mL penicillin, 100 µg/mL streptomycin.

7. Lipofectamine™ 2000 *Transfection Reagent* (Invitrogen).
8. PolyFect Transfection Reagent (Qiagen).

2.2. Cell Culture Material

1. 12-well Multidish (e.g., Nunclon™Δ, NUNC).
2. 18 mm coverslips (e.g., Thermo CB00180RA1).

2.3. Staining Reagents

1. PBS → 10 mM $NaPO_4$ pH 7.4.
2. 4% PFA → 4% PFA in PBS.
3. Permeabilization buffer pH 7.4 → PBS, 0.25% Triton X-100.
4. Blocking buffer → PBS, 2% Glycine, 2% BSA, 0,2% Gelatine, 50 mM NH_3Cl, pH 7.4.
5. ProLong® Gold Antifade Reagent (Molecular Probes).

2.4. Staining Material

1. Forceps with angled tip (e.g., Dumont #5/45).
2. Microscope slides 3 × 1 in. (e.g., Diagonal, 360 535 00).
3. Chipboard slide folder (e.g., Ceesem, 51.850043).
4. Parafilm "M" (Pechiney Plastic Packaging).
5. Lightproofed, humidified chamber (Tables 1 and 2).

Table 1
Primary antibodies

Antigen	Host	Dilution	Company
Bassoon	ms	1:800	Stressgene
Homer 1	rb	1:500	SynapticSystems
Calneuron-1	rb	1:400	Homemade, affinity purified
β-Tubulin III	ms	1:800	Sigma

See Notes 8 and 9

Table 2
Secondary antibodies

Antigen	Host	Dilution	Company
ATTO 647N anti-Rabbit IgG	Goat	1:200	Active Motif
Chromeo™ 494 anti-Mouse IgG	Goat	1:50	Active Motif

See Note 5

3. Methods

3.1. Transfection of Hippocampal Primary Culture with Lipofectamine2000

1. Exchange of media: Rat hippocampal primary neurons are prepared at embryonic day 18 and plated on 18 mm coverslips coated with poly-d-lysine at density 30,000 cells per 1 mL of media as described previously (21). For transfection the conditioned NB+-media, where the neurons were growing until day in vitro 8 (DIV8), has to be replaced by 1 mL of freshly prepared NB– (without the antibiotics). The old media is collected and stored in a Falcon tube in the incubator.
2. Preparation of transfection mix: Transfection is done using 2 µl Lipofectamine2000-reagent and 2 µg of a Caldendrin-EGFP construct (in pEGFP-N1 vector) for each well. Both components are diluted and incubated separately for 5 min in 50 µl Optimem at room temperature (RT). The Lipofectamine2000 containing Optimem is then mixed with the DNA followed by another 20 min of incubation (RT).
3. Transfection of neurons: After the addition of the transfection mix the neurons are transferred back to the incubator where they are kept at 5% CO_2 and 37 °C for another 2 h. Finally the NB–/Optimem transfection mix is replaced by the conditioned media collected prior to transfection and the cells are left in the incubator till DIV16.

3.2. Transfection of HeLa- and COS-7 Cell Cultures with Polyfect

In contrast to the transfection of neurons, an exchange of media prior to transfection is not required. About 24 h after splitting, the cells are ready for transfection. In this approach a double transfection with untagged Calneuron-1 construct (in pcDNA3.1) and GFP-Monomeric-Golgi (subcloned from pDsRed-Monomer-Golgi in frame with EGFP-N1/Clontech) is performed. Therefore, 1.5 µg of each construct (in total 3 µg/well) and 6 µl of Polyfect-reagent are added to 100 µl of RT DMEM– media and kept for 10 min incubation at RT. To the preincubated mix, 100 µl of 37 °C DMEM+ media is added. The transfection mix is then applied to the DMEM+ cultivation media of the cells, which are then kept for another 48 h in the incubator followed by the fixation.

3.3. Staining of Cell Cultures on 18 mm Coverslips for STED-Microscopy

1. Fixation of the cells: Hippocampal primary neurons, HeLa and Cos-7 cells are fixed using 4% paraformaldehyde (PFA). After removal of the cultivation media, cells are kept for 10 min at RT with 4% PFA, followed by three times washing with PBS. The fixation should be carried out in the cultivation plates, whereas for the following steps, the coverslips have to be transferred to a piece of Parafilm placed on microscope slides in a humidified, lightproofed chamber.

2. Permeabilization of the cells: To permeabilize the cells, 150 µl permeabilization buffer is applied to each coverslip. The permeabilization is stopped after 8 min RT incubation, by another three times PBS wash.
3. Blocking and primary antibody labeling: To avoid unspecific binding of the primary antibody the cells are blocked for 1 h at RT in blocking buffer. During the blocking step, dilutions of the primary antibody are prepared in blocking buffer (50 µl per coverslip). To reduce the amount of antibody used for the staining, incubation is carried out putting the coverslips in invers orientation to the antibody solution. The incubation with the primary antibody is performed overnight at 4 °C (see Notes 8 and 9).
4. Secondary antibody labeling: After removal of the primary antibody the coverslips are flipped back and washed five times with PBS. In the meanwhile, dilutions of the fluorescence-labeled secondary antibodies are prepared in blocking buffer. For Ti-Saphir-STED-imaging secondary antibodies tagged with Chromeo 494 and Atto 647N dyes are strongly recommended at dilutions of 1:50 and 1:200, respectively. Keep in mind: To maintain the stability of the fluorophores, it is required to reduce the exposure of them to light to a minimum. After washing, secondary antibody dilutions are applied analogous to the primary antibodies, whereas the incubation is carried out only for 2 h at RT, followed by another five times of washing (see Notes 5 and 6).
5. Embedding: Finally the stained coverslips have to be mounted on microscope slides. To avoid any steric problems while examining the cells on a microscope, it is advisable to put only one coverslip on each slide. Therefore, a drop of RT Prolong-reagent has to be put in the center of the slide in which the coverslip, after a short rinse in distilled water (to remove any salt precipitations), gets finally flipped. After embedding and labeling of the slides, it is best to store them at RT in a light sealed chipboard slide folder. 24 h After embedding, the cells are ready for microscopy (see Note 7).

3.4. Image Acquisition of Stained Cell Cultures by STED-Microscopy

For STED-imaging of Chromeo 494 and Atto 647N dyes (see Fig. 3, Note 5) with emission maxima around 600 nm (channel 1) and 680 nm (channel 2), respectively, we used a commercial 2-channel STED microscope from Leica Microsystems, Germany (see Notes 1–4). Since the Leica STED microscope is fully software controlled, acquiring STED images is nearly as easy as confocal imaging. The following workflow protocol gives an overview about the critical steps and different approaches to acquire high-resolution images.

1. After switching on microscope, computer, scanner, lasers, and starting the LAS software open the configuration menu/laser and activate the multi-photon (MP) laser, the pulsed 532 and 640 nm laser, the 594 nm laser, and the Argon laser (if required for triple labeling in confocal mode). Open the shutter of the MP laser (red light is visible) (see Note 4).
2. Let the system and the MP laser warm up for at least 1 h to ensure mode lock and to stabilize focus and the optical components (from thermal drift).
3. Make sure that the 100× Oil Plan Apo NA 1.4 STED objective is inserted into the beam path.
4. Open configuration menu/STED and let the auto alignment routine run, which takes only few minutes. This routine optimizes the adjustment between the excitation lasers and the STED laser and should be repeated every 2 h in order to minimize thermal drifts within the beam paths. Because the sample is not illuminated during the beam alignment, there is no need to remove it from the microscope stage.
5. Since Chromeo 494 and Atto 647 N emit their fluorescence in the red range of the spectrum (Fig. 3), it is difficult to find an area of interest by eye with wide field epifluorescence illumination. Therefore, it is advisable to have a third label, like GFP or Alexa 488, within the sample that helps to find the focus and to navigate on the sample until one has found the region of interest for STED imaging (see Note 5).
6. Before scanning the best position one should perform a test run with a dispensable structure to find the optimized settings without bleaching the significant areas from which STED images should be acquired. In contrast to Chromeo 494 with low quantum yield Atto 647N is a rather stable fluorophore that allows repeated scanning. Hence, it is recommendable to use the Atto 647N channel for fine adjustments at higher zoom factors (see Note 5).
7. Confocal as well as STED images are recorded sequentially by scanning the focused beam with a galvo-mirror across the specimen.

   A typical image series consists of four channels, which have to be acquired in sequential mode. Channel 1: Atto 647N (LSM mode), channel 2: chromeo 494 (LSM mode), channel 3: Atto 647N (STED mode), channel 4: Chromeo 494 (STED mode). Eventually in a 5th channel GFP or Alexa 488 can be recorded as counterstaining in LSM mode (see Notes 2, 3 and Figs. 4–8).
8. Atto 647N and Chromeo 494 have to be captured by Avalanche photodiodes (APDs), whereas the counterstaining

(i.e., GFP or Alexa 488) should be imaged by one of the internal photomultiplier tubes (PMTs).

9. Adjusting the scan parameters according to the signal to noise ratio within the sample requires fine adjustment of each channel while scanning. To avoid bleaching fast scanning (1,000 Hz) is recommended at low resolution (256×256 pixel) with a look up table (glow over/under) that indicates saturated pixel in blue and background values in green.
10. To find the optimal intensity of the excitation laser start scanning in LSM mode and then toggle between LSM and STED mode by activating the button at the STED slider. Increasing the power of the STED laser should result in higher depletion, visible as smaller structures indicating improvement of resolution. Care must be taken to avoid bleaching from strong laser excitation as well as re-excitation from the depletion laser (see Notes 1–3).
11. If no clear improvement between the STED and the LSM image is visible the beam alignment has to be controlled. If excitation and depletion lasers are well aligned a missing STED effect might also be caused by a mismatch in the temporal synchronization between excitation and STED laser pulse. In this case the default value of the delay time between both pulses has to be tested manually in the configuration/STED menu.
12. Once optimal settings for the individual channels have been found, they can be taken over with slight adaptation for a whole series of images. For high-quality STED recording, two opposite strategies can be applied: Either the scan speed can be reduced to 10, 100 or 200 Hz with no or little averaging (4× is a good value) or the scan speed is set to 1,000 or 1,400 Hz and the image is averaged up to 64 times. With both settings we have obtained reasonable results, if the staining is homogeneous without any hot spots in the sample. Because APDs are very sensitive but lack high dynamic range as known from PMTs, they will shut off immediately after attaining saturation. Since the risk of entering saturation is much higher with lower scanning speed, a repetition rate of 1,000 Hz and 64 times line averaging is recommend as optimal scanning parameters.
13. In contrast to the 532 nm excitation laser, which is controlled by an AOTF, the intensity of the pulsed 640 nm laser has to be adjusted manually before channels toggle between LSM (intensity value at the power supply: 5.25) and STED (Intensity value: 5.3) mode. For this reason it is advised to scan alternating with 532 and 640 nm excitation.
14. To avoid undersampling and thus loss of information, STED imaging requires a pixel size below 30 nm. This is important, because due to the Nyquist theorem, the sampling frequency

should be at least two times higher than the highest spatial frequencies in the sample. Practically it means that an adequate data representation is fulfilled if the pixel size is two to three times below the theoretical resolution. In STED mode, a pixel size of 25 nm is achieved with an 100× Oil NA 1.4 objective at an image format of 1,024 pixel with a zoom factor of 6.

15. Acquisition of 3D stacks is principally possible with the STED system, but one has to take into account that the axial resolution of the commercial setup is still the same as in confocal mode (500–700 nm). Moreover, repeated scanning boosts bleaching, particularly of the Chromeo 494 dye. To minimize bleaching during stack acquisition fast scanning (1,400 or 8,000 Hz using the resonant scanner) in combination with enhanced averaging (i.e., 64× line average) is strongly recommended.

3.5. Image Processing

To improve image quality raw data of confocal and STED images are deconvolved using Autoquant deconvolution software (Media Cybernetics, Inc., Bethesda, USA) with a theoretical PSF. Subsequently, images are processed using ImageJ (National Institutes of Health, USA) for merging channels and conversion into 8 Bit RGB images. Contrast and brightness levels of individual channels are finally adapted by Photoshop CS 5 (Adobe. System, Inc., San Jose, USA).

4. Notes

1. Spontaneous versus stimulated emission. In fluorescence microscopy the process of absorption and emission can be described as cycle between lower (ground) or higher (excited) electronic energy states of an atom. If the atom absorbs a photon of a certain frequency ν (that equals the energy difference between the two states) an electron makes a transition to the excited electronic state (Fig. 2, left panel). From here it will relax back spontaneously to the ground state after a short period of time (i.e., the fluorescence lifetime) by emitting a photon of less energy (i.e., red-shifted wavelength). Mathematically, the energy difference between the excited (E2) and the ground (E1) state is given by the equation:

$$E2 - E1 = h\nu,$$

where ν is the frequency and h is Planck's constant. Typical excited state lifetimes of fluorescent dyes are in the range of picoseconds to nanoseconds.

In contrast to spontaneous relaxation stimulated (or induced) emission occurs when an electron in the excited state encounters a photon whose energy matches the difference between the electron's energy and the ground state (Fig. 2 center panel). In this case the photon will stimulate the electron to return immediately to the lower energy state by emitting an additional photon of the same phase, frequency, direction, and polarization, as the incident photon. Stimulated emission was theoretically predicted first by Albert Einstein in 1917 (35). It can be used to augment the external field (as in lasers) or to deplete spontaneous fluorescence specifically by switching fluorescent molecules off in a certain area as in STED microscopy (Figs. 1 and 2 right panel).

2. Resolution limit in confocal microscopy. In confocal laser scanning microscopy, the excitation beam is focused by an objective into a diffraction limited spot, which is sequentially moved across the specimen by a scanning mirror. The emitted fluorescence is then collected through the objective and guided to a detector (usually a photomultiplier tube (PMT)). The light distribution of the focal spot is determined by the point-spread function (PSF) which, in an ideal case, shows a typical pattern called "Airy disk." Its smallest size is defined by the diffraction limitation of light. The diffraction limitation was first described by Ernst Abbe in 1873 (34) in his formula:

$$d = \frac{\lambda}{2n \sin\alpha}$$

where d is the resolvable characteristic value, λ is the wavelength, n is the refractive index of the medium, and $\sin\alpha$ the semi-aperture angle of the objective. Because of this resolution barrier the excitation spot for illuminating fluorescent structures in a scanning microscope cannot be smaller than approximately half the wavelength of visible light, i.e., for blue excitation: »200 nm.

3. Resolution in STED microscopy. In a scanning STED (STimulated Emission Depletion) microscope Abbe's resolution limit is circumvented by annihilating excited dye molecules in the periphery of the excitation spot, thus confining the fluorescence emission to a smaller area in the center. The STED concept of deactivating dye molecules was first described in 1994 by Stephan Hell (30). In a scanning microscope, it is realized by modulating the wavefront of a second red-shifted laser with a patterned phase plate (vortex pattern), so that a doughnut shaped ring around the excitation spot is illuminated. As effect the fluorescence emission of excited molecules is increasingly quenched in the outer rim by the second (STED)

laser, whereas the emission in the center of the excitation spot is widely unaffected (Figs. 1 and 2 right panel). In principal, excitation and quenching can be done by cw- or pulsed lasers, respectively. Whereas cw-lasers are cheaper than pulsed lasers and require only a precise spatial alignment between excitation and quenching beams, pulsed lasers are more complex and necessitate, in addition to the spatial alignment, a precise temporal cyclic succession of both excitation and de-excitation laser pulses to assure that the arrival of both pulse trains are precisely synchronized. Using powerful depletion lasers forces almost all of the excited molecules in the outer ring to revert to the ground state, leaving only a tiny fraction of excited molecules in the center region of the excitation spot the chance to fluoresce. In other words, the size of the scanning spot from where fluorescent emission can be detected is defined by the precise arrival and the intensity of the de-excitation beam, i.e., the higher the depletion power, the smaller the fraction of fluorescent molecules in the remaining central spot and the better the resolution. Mathematically, the resolution improvement beyond the diffraction limit is described by the following extension of Abbe's formula:

$$d = \frac{\lambda}{2n \sin\alpha \sqrt{(1 + \frac{I}{I_s})}}$$

where I is the intensity of the STED laser and I_s the saturation intensity of the selected fluorophore, i.e., the laser intensity at which the fluorescence depleted by 50% (22).

4. Configuration of the 2 channel STED setup. Figure 1 shows a scheme of a Titanium Sapphire laser-based STED microscope used for imaging dyes with emission maxima between 600 and 700 nm. For 2 channel excitation, diode lasers (PicoQuant, Berlin) emitting pulses of ≈70 ps at 532 nm (channel 1) and 640 nm (channel 2) with a repetition rate of 80 MHz were used. The STED pulses of 750–760 nm (repetition rate of 80 MHz) were generated by the Ti-Sapphire laser (Cameleon Ultra II, Coherent Inc., Santa Clara, USA) that provided also the triggering signal for the precise synchronization of the STED laser with the excitation lasers. Temporal adjustment of excitation and quenching pulses was managed via a delay unit to guarantee that every excitation pulse is immediately followed by a depletion pulse. The STED laser pulses of ≈100 fs were first prestretched to ≈1 ps by guiding the beam through a glass block and then stretched to ≈300 ps via a 100 m long polarization-maintaining glass fiber. Subsequently, the collimated STED beam was guided through a vortex

Table 3
Photophysical properties of STED dyes

Dye	Abs (nm)	Em (nm)	ε (M^{-1} cm^{-1})	QY	Stoke's shift (nm)
ATTO 647N	644	669	150,000	65	25
Chromeo 494	494	628	55,000	7[a]/25[b]	134

Abs absorption maximum in water, *Em* emission maximum in water, ε molar extinction coefficient, *QY* quantum yield, *Stoke's shift* Em-Abs
[a]Goat–anti-mouse conjugate or Goat–anti-rabbit conjugate
[b]BSA-conjugate

patterned phase plate and then overlaid with the excitation beams via a dichroic mirror. Calibration between excitation and STED pulse is done automatically by an alignment tool provided by the software. Both beams were focused into the sample by a 100× Pl APO objective (Leica-Microsystems, Wetzlar, Germany), and the emitted fluorescence signal was registered by two avalanche photon diodes (APDs, Perkin Elmer, Inc., San Jose, USA). To enhance focus stability and minimize thermal drift, the microscope was equipped with light tight customized heatable incubation chamber (Pecon, Erbach, Germany).

5. Dyes used for STED microscopy. Although principally almost all fluorophores can be depleted by stimulated emission, practically the photophysical properties, particularly the photostability, and the available laser lines for pulsed excitation shrink dramatically the number of fluorophores to be considered suitable. A list of dyes recommended for cw-STED and/or Ti-Sapphire STED microscopy can be found online at http://nanobiophotonics.mpibpc.mpg.de/old/dyes/. In our hands the best results, so far, were obtained with Atto 647N (Atto-Tec, Siegen, Germany) excited at 640 nm (Fig. 3 center panel). For co-localization studies, Chromeo 494 (Active Motif Chromeon GmbH, Tegernheim, Germany), excited at 532 nm, was used as second STED-fluorophore (Fig. 3 left) in association with Atto 647 N (Fig. 3 right panel). Due to the large Stoke's shift of Chromeo 494 this dye has a low quantum efficacy and care must be taken to avoid fast bleaching (see Table 3). Both immunostainings could be combined with previous transfection of genetically encoded fluorophores, like eGFP, without considerable crosstalk. The latter can be used as third label to define cell borders or areas of interest and recorded in confocal mode only.
6. Direct versus indirect labeling. Since the size and the number of the fluorophores linked to an antibody influence the

dimensions of the structure to be recorded, direct labeling of primary-antibodies is advised. Compared to indirect immune-fluorescence with directly labeled antibodies, the fluorophore is considerably closer to the structure of interest, thereby contributing to an improvement of the resolution. However, a drawback of direct immune-fluorescence is an attenuation of signal due to less fluorophores.

7. Embedding and mounting. STED images are acquired by selected high numerical aperture objectives (100× Plan Apo 1.4 NA oil), which are designed to be used with coverslips of 170 µm thickness and on the assumption that also the refractive indices of embedding and immersion media equal $n = 1.52$. Since any mismatch in the refractive index of the beam path will dramatically reduce the resolution, care must be taken that the embedding medium of the sample, the coverslip, and the immersion medium do not alter the refractive index perceptibly. Hence, for super-resolution microscopy we recommend the usage of immersion oil from Zeiss or Leica (F-518) with a refractive index of 5.18 and coverslips with a homogeneous thickness (170 µm ± 5 µm), like from Zeiss # 1.5 (Carl Zeiss, Jena, Germany) or Marienfeld No 1.5H (http://www.marienfeld-superior.com).

   As embedding medium in combination with an antifade reagent, we have some good experience with Mowiol + Dabco (1,4-Diazabicyclo-octane) in Glcyerol/Tris-buffer, pH 8.5. Mowiol (Mowiol 4.88, Calbiochem) is a solution of polyvinyl alcohol, which hardens overnight after slide preparation, and does not require the coverslips to be sealed with nail varnish. The addition of Dabco or *p*-Phenylenediamine (PPD) is recommended to reduce bleaching of fluorescent probes. A protocol for Mowiol preparation is presented at http://www.niaid.nih.gov/LabsAndResources/labs/aboutlabs/rtb/biologicalImaging/protocols/Pages/mowiolPreparation.aspx.
   An alternative Glycerol-based mounting medium used for STED-imaging is ProLong Gold (Invitrogen). Prolong Gold is suitable for Atto 647N and Chromeo 494 but not so good for eGFP and other fluorescent proteins. With time it polymerizes so that a sealing is not necessary. A good overview about mountants and antifades can be found at http://www.biocenter.helsinki.fi/bi/lmu/images/Mountants.pdf.

   As non-hardening mounting medium with antioxidant features we have successfully applied TDE (2,2 -Thiodiethanol, Sigma Aldrich). TDE allows a fine adjustment of the refractive index between water (1.33) and oil (1.52) by changing the ratio between water and TDE in the mixture of an ascending series (36).

8. Primary antibodies used for presynaptic staining. To demonstrate the potential of STED imaging for the subcellular

localization of calcium-binding proteins in neurons, we performed immunostainings against pre- and postsynaptic scaffolding proteins in hippocampal cell cultures previously transfected with a GFP-fusion construct of Caldendrin (Figs. 6–8). As presynaptic marker, we chose Bassoon, a giant protein of 420 kDa, which is supposed to be a major constituent of the so-called cytomatrix at the active zone found at both excitatory and inhibitory synapses (37–40). Ultrastructural and immunocytochemical studies have shown that Bassoon is always present in nascent synapses, indicating that it plays an essential role during assembly of active zones. Here, we recognized Bassoon by a monoclonal antibody followed by indirect immune-fluorescence with Chromeo 494 as dye.

9. Primary antibodies used for postsynaptic staining. As postsynaptic marker we chose Homer, which consists of several isoforms (Homer-1, 2, 3) and is localized at the postsynapse of excitatory synapses (41). It acts as an adaptor protein to link multiple targets, such as type 1 metabotropic glutamate receptors, IP3 receptors, ProSAP/Shanks, and others (42–44). By inducing the clustering of these proteins, Homer was suggested to organize distinct signaling pathways and to modulate calcium signaling and dendritic spine morphology (45). In our study, Homer was identified by an affinity-purified rabbit antibody against Homer-1 that was visualized by anti-rabbit Atto 647N. Caldendrin-GFP expressed in adult hippocampal primary neurons was unevenly filling up complete neurons with most of GFP fluorescence in the soma (but not the nucleus), dendrites and dendritic spines (Figs. 6–8).

Acknowledgments

This work was supported by the following grants: BMBF "Novel Optics" VDI 13N10077 and DFG SFB 854 TPZ (WZ) and DFG Kr1879/3-1 and SFB 854 TP7 (MK).

References

1. Berridge MJ, Bootman MD, Lipp P (1998) Calcium—a life and death signal. Nature 395:645–648
2. Berridge MJ, Bootman MD, Roderick HL (2003) Calcium signalling: dynamics, homeostasis and remodelling. Nat Rev Mol Cell Biol 4:517–529
3. Pozzo-Miller LD, Pivovarova NB, Leapman RD et al (1997) Activity-dependent calcium sequestration in dendrites of hippocampal neurons in brain slices. J Neurosci 17: 8729–8738
4. Mikhaylova M, Hradsky J, Kreutz MR (2011) Between promiscuity and specificity: novel roles of EF-hand calcium sensors in neuronal Ca2+ signalling. J Neurochem 118:695–713
5. Ikura M, Ames JB (2006) Genetic polymorphism and protein conformational plasticity in

the calmodulin superfamily: two ways to promote multifunctionality. Proc Natl Acad Sci U S A 103:1159–1164

6. Burgoyne RD (2007) Neuronal calcium sensor proteins: generating diversity in neuronal Ca^{2+} signalling. Nat Rev Neurosci 8:182–193
7. Fries R, Reddy PP, Mikhaylova M et al (2010) Dynamic cellular translocation of caldendrin is facilitated by the Ca2+-myristoyl switch of recoverin. J Neurochem 113:1150–1162
8. McCue HV, Burgoyne RD, Haynes LP (2009) Membrane targeting of the EF-hand containing calcium-sensing proteins CaBP7 and CaBP8. Biochem Biophys Res Commun 380: 825–831
9. McCue HV, Burgoyne RD, Haynes LP (2011) Determination of the membrane topology of the small EF-Hand Ca^{2+}-sensing proteins CaBP7 and CaBP8. PLoS One 6:e17853
10. Mikhaylova M, Reddy PP, Munsch T et al (2009) Calneurons provide a calcium threshold for trans-Golgi network to plasma membrane trafficking. Proc Natl Acad Sci USA 106:9093–9098
11. Hradsky J, Raghuram V, Reddy PP et al (2011) Post-translational membrane insertion of tail-anchored transmembrane EF-hand Ca2+ sensor Calneurons requires the TRC40/Asna1 protein chaperone. J Biol Chem 286:36762–36776
12. Mikhaylova M, Reddy PP, Kreutz MR (2010) Role of neuronal Ca2+-sensor proteins in Golgi-cell-surface membrane traffic. Biochem Soc Trans 38:177–180
13. Shih PY, Lin CL, Cheng PW et al (2009) Calneuron I inhibits Ca^{2+} channel activity in bovine chromaffin cells. Biochem Biophys Res Commun 388:549–553
14. Seidenbecher CI, Langnaese K, Sanmartí-Vila L et al (1998) Caldendrin, a novel neuronal calcium-binding protein confined to the somato-dendritic compartment. J Biol Chem 273:21324–21331
15. Laube G, Seidenbecher CI, Richter K et al (2002) The neuron-specific Ca^{2+}-binding protein caldendrin: gene structure, splice isoforms and expression in the rat central nervous system. Mol Cell Neurosci 19:459–475
16. Bernstein HG, Seidenbecher CI, Smalla KH et al (2003) Distribution and cellular localization of caldendrin immunoreactivity in adult human forebrain. J Histochem Cytochem 51:1109–1112
17. Smalla KH, Seidenbecher CI, Tischmeyer W et al (2003) Kainate-induced epileptic seizures induce a recruitment of caldendrin to the postsynaptic density in rat brain. Brain Res Mol Brain Res 19:159–162
18. Mikhaylova M, Sharma Y, Reissner C et al (2006) Neuronal Ca^{2+} signaling via caldendrin and calneurons. Biochim Biophys Acta 1763:1229–1237
19. McCue HV, Haynes LP, Burgoyne RD (2010) The diversity of calcium sensor proteins in the regulation of neuronal function. Cold Spring Harb Perspect Biol 2. doi:10.1101/cshperspect.a004085
20. Seidenbecher CI, Landwehr M, Smalla KH et al (2004) Caldendrin but not calmodulin binds to light chain 3 of MAP1A/B: an association with the microtubule cytoskeleton highlighting exclusive binding partners for neuronal Ca^{2+}-sensor proteins. J Mol Biol 336:957–970
21. Dieterich DC, Karpova A, Mikhaylova M et al (2008) Caldendrin-Jacob: a protein liaison that couples NMDA receptor signalling to the nucleus. PLoS Biol 6:e34, Erratum in: PLoS Biol. 7 (2009):e1000022
22. Hell SW (2007) Far-field optical nanoscopy. Science 316:1153–1158
23. Hell SW, Stelzer EHK, Lindek S et al (1994) Confocal microscopy with an increased detection aperture: type-B 4Pi confocal microscopy. Opt Lett 19:222–224
24. Gustafsson MG (2000) Surpassing the lateral resolution limit by a factor of two using structured illumination microscopy. J Microsc 198: 82–87
25. Gustafsson MG (2005) Nonlinear structured-illumination microscopy: wide-field fluorescence imaging with theoretically unlimited resolution. Proc Natl Acad Sci USA 102: 13081–13086
26. Heintzmann R, Cremer C (1999) Lateral modulated excitation microscopy: improvement of resolution by using a diffraction grating. Proc SPIE 3568:185–196
27. Esa A, Edelmann P, Kreth G et al (2000) Three-dimensional spectral precision distance microscopy of chromatin nanostructures after triple-colour DNA labelling: a study of the BCR region on chromosome 22 and the Philadelphia chromosome. J Microsc 199: 96–105
28. Lemmer P, Gunkel M, Baddeley D et al (2008) SPDM: light microscopy with single-molecule resolution at the nanoscale. Appl Phys B 93: 1–12
29. Hell SW, Kroug M (1995) Ground-state-depletion: a concept for breaking the diffraction resolution limit. Appl Phys B 60: 495–497
30. Hell SW, Wichmann J (1994) Breaking the diffraction resolution limit by stimulated emission. Opt Lett 19:780–782

31. Klar TA, Hell SW (1999) Subdiffraction resolution in far-field fluorescence microscopy. Opt Lett 24:954–956
32. Betzig E, Patterson GH, Sougrat R et al (2006) Imaging intracellular fluorescent proteins at nanometer resolution. Science 313:1642–1645
33. Rust MJ, Bates M, Zhuang X (2006) Sub-diffraction-limit imaging by stochastic optical reconstruction microscopy (STORM). Nat Methods 3:793–795
34. Abbe E (1873) Beiträge zur Theorie des Mikroskops und ihrer mikroskopischen Wahrnehmung. Arch Mikrosk Anat 9:411–468
35. Einstein A (1917) Zur Quantentheorie der Strahlung. Physik Zeitschr 18:121–128
36. Staudt T, Lang MC, Medda R et al (2007) 2,2 -thiodiethanol: a new water soluble mounting medium for high resolution optical microscopy. Microsc Res Tech 70:1–9
37. Cases-Langhoff C, Voss B, Garner AM et al (1996) Piccolo, a novel 420 kDa protein associated with the presynaptic cytomatrix. Eur J Cell Biol 69:214–223
38. Tom Dieck S, Sanmartí-Vila L, Langnaese K et al (1998) Bassoon, a novel zinc-finger CAG/glutamine-repeat protein selectively localized at the active zone of presynaptic nerve terminals. J Cell Biol 142:499–509
39. Dresbach T, Hempelmann A, Spilker C et al (2003) Functional regions of the presynaptic cytomatrix protein bassoon: significance for synaptic targeting and cytomatrix anchoring. Mol Cell Neurosci 23:279–291
40. Richter K, Langnaese K, Kreutz MR et al (1999) Presynaptic cytomatrix protein bassoon is localized at both excitatory and inhibitory synapses of rat brain. J Comp Neurol 408:437–448
41. Dani A, Huang B, Bergan J et al (2010) Superresolution imaging of chemical synapses in the brain. Neuron 68:843–856
42. Brakeman PR, Lanahan AA, O'Brien R et al (1997) Homer: a protein that selectively binds metabotropic glutamate receptors. Nature 386:284–288
43. Yuan JP, Kiselyov K, Shin DM et al (2003) Homer binds TRPC family channels and is required for gating of TRPC1 by IP3 receptors. Cell 114:777–789
44. Tu JC, Xiao B, Naisbitt S et al (1999) Coupling of mGluR/Homer and PSD-95 complexes by the Shank family of postsynaptic density proteins. Neuron 23:583–592
45. Sala C, Piech V, Wilson NR et al (2001) Regulation of dendritic spine morphology and synaptic function by Shank and Homer. Neuron 31:115–130